Molecular Modeling of Micelle Formation and Solubilization in Block Copolymer Micelles. 2. Lattice Theory for Monomers with Internal Degrees of Freedom

Patricia N. Hurter,† Jan M. H. M. Scheutjens,‡,§ and T. Alan Hatton*,†

Department of Chemical Engineering, Massachusetts Institute of Technology, Cambridge, Massachusetts 02139, and Department of Physical and Colloid Chemistry, Wageningen Agricultural University, 6700 EK Wageningen, The Netherlands

Received September 10, 1992; Revised Manuscript Received June 23, 1993

ABSTRACT: A self-consistent mean-field lattice theory of the micellization and solubilization properties of poly(ethylene oxide)–poly(propylene oxide) block copolymers is described. The polymer segments are allowed to assume both polar and nonpolar conformations (corresponding to the gauche and trans rotations of the C–C and C–O bonds), which permits the dependence of the segment–segment interactions on temperature and composition to be accounted for in a physically realistic manner. The phase diagrams of poly(ethylene oxide) and poly(propylene oxide) in water, both of which exhibit lower critical solution temperatures, can be reproduced semiquantitatively. The predictions of the theory compare favorably with published light scattering results on the aggregation behavior of block copolymers and with our experimental results for the solubilization of naphthalene in these micelles as a function of polymer composition and molecular weight. The dependence of the micelle–water partition coefficient on polymer composition is not simply related to the proportion of the hydrophobic constituent but depends on the detailed micelle structure. The strong effect of the molecular weight and PPO content of the polymer on the amount of naphthalene solubilized observed experimentally was interpreted in terms of the model results.

Introduction

The formation of micelles in aqueous solutions of block copolymers and their ability to enhance significantly the solubility of hydrophobic solutes in these solutions have many important industrial and biomedical applications. For the rational selection and design of appropriate block copolymers for any given application, it is desirable to have an appreciation of the effects of polymer architecture, solution conditions, and solute properties on the structure and solubilization capacity of these micellar systems. This must depend to a large extent on the availability of good experimental studies and of sound theoretical models to enable extrapolation to conditions beyond those for which experimental data are available; this modeling of block copolymer micelle formation and solubilization ability is the topic of the present paper.

Recently, light scattering and intrinsic viscosity measurements have shed some light on the effect of temperature on the aggregation behavior of poly(ethylene oxide)–poly(propylene oxide) (PEO–PPO) block copolymers. It is generally evident that these polymers do not form micelles at low temperatures, exhibit micellar growth at intermediate temperatures, and yield micelles of constant size at higher temperatures.[1–6] Zhou and Chu,[6] for instance, detected three temperature regions, which they called the unimer, transition, and micelle regions, respectively. At low temperatures, particles with a broad polydispersity were detected. At higher temperatures, however, micelle molecular weights were found to increase linearly with temperature, while the hydrodynamic radius remained constant. It was suggested that the constant micelle size accompanying an increase in the aggregation number in the micelle region was due to exclusion of water from the micelle interior with an increase in temperature. The results of Brown et al.[3] suggested that monomers, micelles, and micellar aggregates coexist, the relative proportions of each species depending strongly on temperature and polymer concentration. It is apparent that polymers which are relatively less hydrophobic, due to either a high ethylene oxide content or a low molecular weight, do not form micelles at room temperature but do start to aggregate at higher temperatures, closer to the cloud point of the polymer in water. This can be explained by the fact that water becomes a poorer solvent for ethylene oxide at higher temperatures, and these polymers thus have an increased tendency to aggregate and form micelles as the temperature of the solution increases. The more hydrophobic polymers exhibit a similar behavior, except that micellar formation can begin at temperatures well below room temperature.

The solubilization characteristics of polycyclic aromatic hydrocarbons in block copolymer micelles of poly(ethylene oxide)–poly(propylene oxide) studied recently by Hurter and Hatton[7,8] are consistent with the results of these light scattering studies. The partition coefficient between the micelles and bulk water phase was constant for the more hydrophobic polymers and those of higher molecular weight but depended on polymer concentration with the lower molecular weight polymers.[7] In certain temperature regions, the solubilization increased with increasing temperature, consistent with the growth of micelles, but leveled off at the higher temperatures.[9] The transition temperatures were lower for the more hydrophobic polymers.

Block copolymer micelle formation and solubilization behavior have been modeled using a self-consistent mean-field lattice theory.[8,10] The simple lattice theory for flexible-chain molecules presented in these works, however, cannot capture effects such as the phase behavior of poly(ethylene oxide) and poly(propylene oxide) in water, where a lower critical solution temperature is observed. To predict such behavior, the gauche and trans bond orientations of the polymer chain must be accounted for: Leermakers and Scheutjens[11] used the rotational isomeric state scheme to accommodate these orientations and eliminate backfolding, combined with the self-consistent-

* Author to whom all correspondence should be addressed.
† Massachusetts Institute of Technology.
‡ Wageningen Agricultural University.
§ Deceased, August 2, 1992.

0024-9297/93/2226-5030$04.00/0

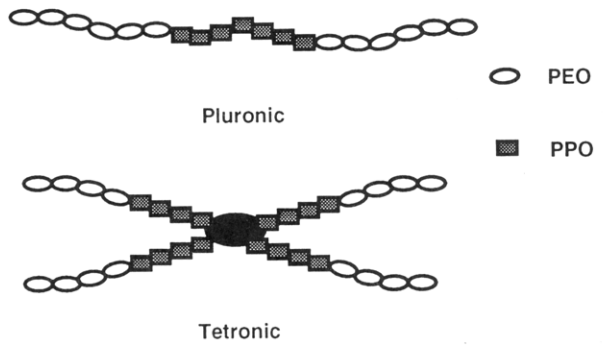

Figure 1. Schematic diagram of the BASF Pluronic and Tetronic block copolymers.

Table I. Properties of the Polymers Modeled[a]

title	modeled as:	PEO content (wt %)	mol wt
P103	$EO_{20}PO_{61}EO_{20}$	30	4950
P104	$EO_{30}PO_{61}EO_{30}$	40	5900
P105	$EO_{42}PO_{61}EO_{42}$	50	6500
P106	$EO_{50}PO_{61}EO_{50}$		
L64	$EO_{13}PO_{29}EO_{13}$	40	2900
P84	$EO_{20}PO_{41}EO_{20}$	40	4200
P94	$EO_{25}PO_{51}EO_{25}$		

[a] The P106 and the P94 are "hypothetical" polymers; the remaining polymers model Pluronic polymers available from BASF Corp.

field theory, to predict the formation of lipid bilayer membranes and lipid vesicles. The lower critical solution temperature of PEO in water was modeled by Barneveld,[12] who took the PEO molecule to be a copolymer with alternating polar and nonpolar segments and allowed the Flory–Huggins χ parameters to decrease with increasing temperature.

An approach which is computationally simpler than the rotational isomeric state scheme, but which still accounts for the temperature and composition dependence of χ in a physically realistic manner, has recently been presented by Karlstrom.[13] This model for PEO recognizes that certain sequences of the gauche–trans orientations in a PEO monomer will lead to polar conformations, while others will be essentially nonpolar. The polar conformations are energetically favored, while the nonpolar conformations have a higher degeneracy. Consequently, as the temperature is increased, the fraction of monomers assuming the nonpolar conformation increases, which leads to water becoming a poorer solvent for PEO. Using this model, the solubility gap in PEO–water and PPO–water phase diagrams can be reproduced.

In this paper, a model for solubilization in block copolymer micelles is presented, which incorporates Karlstrom's ideas to account for these conformational distributions in PEO and PPO and allows the investigation of temperature effects on the aggregation behavior of block copolymers and the solubilization of hydrophobic solutes in micelles formed by these polymers. The polymers modeled simulate the triblock Pluronic and branched Tetronic range of block copolymers of PEO and PPO, manufactured by BASF Corp., which are illustrated schematically in Figure 1. Table I lists the physical properties of the polymers discussed in this paper. Linse and co-workers,[14,15] in an independent study, have also used this approach to probe the effects of temperature and block copolymer architecture on the formation of PEO–PPO block copolymer micelles, but in the absence of any solutes.

Theory

A detailed description of the self-consistent mean-field lattice theory is given in a companion paper,[8] hereafter referred to as paper 1. In this theory, the polymer chains are allowed to assume various random-walk conformations on a lattice, which for our purposes is considered to be spherical. The interactions between segments within parallel or concentric layers are described by invoking the mean-field approximation in the lateral directions only, so that concentration profiles in the radial direction can be accounted for. Following the derivation presented by Linse and Bjorling,[16] the potential experienced by a segment of type A, $u_A(z)$, is given by

$$\frac{u_A(z)}{kT} = \frac{u'(z)}{kT} + \sum_j^{p,n}\left[P_{Aj}(z)\left(\frac{\tilde{u}_{Aj}}{kT} + \ln\frac{P_{Aj}(z)}{g_{Aj}}\right) - P_{Aj}^{\infty}\left(\frac{\tilde{u}_{Aj}}{kT} + \ln\frac{P_{Aj}^{\infty}}{g_{Aj}}\right)\right] + \sum_B\sum_j^{p,n}\sum_k^{p,n}\chi_{Aj,Bk}\left[P_{Aj}(z)\langle P_{Bk}(z)\,\phi_B(z)\rangle - P_{Aj}^{\infty}P_{Bk}^{\infty}\phi_B^{\infty}\right] \quad (1)$$

The hard-core potential, $u'(z)$, ensures that the constraint of constant density within a lattice layer is satisfied. The summations over B are for all segment types, while those over j or k are for the internal states, represented by p for polar and n for nonpolar, respectively. $P_{Aj}(z)$ is the probability of finding segment A in state j, in layer z, an expression for which is described below. $\tilde{u}_{Aj}$ is the internal energy of segment A in state j (which arises from the difference in energy between the trans and gauche conformations) and g_{Aj} is the degeneration of state j for segment A. The interaction between segments of type A in state j and segments of type B in state k is characterized by $\chi_{Aj,Bk}$, while the angular brackets indicate an averaging of the volume fraction over three adjacent layers, so that

$$\langle\phi_B(z)\rangle = \lambda_{-1}\phi_B(z-1) + \lambda_0\phi_B(z) + \lambda_1\phi_B(z+1)$$

If the internal energies are known, then the free segment distribution function $G_A(z)$, which is the weighting factor for a free segment of type A in layer z, is given by the Boltzmann factor containing the local potential experienced by the segment:

$$G_A(z) = \exp(-u_A(z)/kT) \quad (2)$$

As described in paper 1,[8] the chain connectivity is taken into account by generating a step-weighted random walk. A matrix of end-point distributions is calculated, where $G(z,s|1)$ is the weighting factor for a walk which starts with segment 1 in any layer and ends with segment s in layer z:

$$\mathbf{G} = \begin{bmatrix} G(1,1|1) & \dots & \dots & \dots & G(1,r|1) \\ G(z,1|1) & \dots & G(z,s|1) & \dots & G(z,r|1) \\ G(M,1|1) & \dots & \dots & \dots & G(M,r|1) \end{bmatrix} \quad (3)$$

where $G(z,s|1) = \langle G(z,s-1|1)\rangle G(z,s)$.

A matrix of end-point distributions assuming that segment r is free, i.e., $G(z,s|r)$, can be generated in an analogous manner. The statistical weight of all conformations with segment s in layer z is given by the product of three contributions, the probability of finding segment s-1 in layer z, z-1, or z+1, the probability of finding segment s+1 in one of these layers, and the probability of finding a free segment s in layer z. Thus,

$$G(z,s|1;r) = \langle G(z,s-1|1)\rangle G(z,s)\,\langle G(z,s+1|r)\rangle \quad (4)$$

The volume fraction of segment s in layer z is proportional

to the weighting factor, so that rearrangement leads to

$$\phi(z,s) = c\frac{G(z,s|1)\,G(z,s|r)}{G(z,s)} \tag{5}$$

The proportionality constant c is found by specifying the total amount of polymer in the system, as described in detail in paper 1. The state distribution $P_{Aj}(z)$, which is the probability of finding a segment of type A in state j, in layer z, can be derived explicitly from the partition function, as shown by Linse and Bjorling,[16] and is given by

$$P_{Aj}(z) = X_{Aj}(z)/\sum_{j}^{p,n} X_{Aj}(z) \tag{6}$$

where

$$X_{Aj}(z) = g_{Aj}\exp\left[-\left(\frac{\tilde{u}_{Aj}}{kT} - \sum_{B}\sum_{k}^{p,n}\chi_{Aj,Bk}\langle P_{Bk}(z)\,\phi_B(z)\rangle\right)\right] \tag{7}$$

This equation illustrates the dependence of the balance between the polar and nonpolar conformations on temperature. The ratio of polar to nonpolar states depends on the difference between the internal energies of the two states and on the ratio of their degeneracies. At high temperatures, the energetic advantage of the polar conformation would decrease, resulting in an increase in the fraction of segments in the entropically favored nonpolar conformation, which has a higher degeneracy. This would make water become a poorer solvent for polymers such as PEO and PPO at high temperatures, which offers an explanation for the observed lower critical solution temperature for these polymers.

Using the equations as derived above would involve an extra iteration to find the state probability distributions $P_{Aj}(z)$. A set of internal energies $u_A(z)$ would be assumed, from which the free segment weighting factors $G_A(z)$ could be calculated, and hence also the matrices of end-point distributions and the volume fraction profiles. The probabilities $P_{Aj}(z)$ can be found by solving the implicit set of equations given by eqs 6 and 7, after which an updated set of $u_A(z)$ could be calculated. However, the system can be simplified considerably by substituting eq 7 into eq 1, so that the expression for the potential of a segment of type A becomes

$$u_A(z) = u'(z) - kT\ln\left(\frac{X_{Ap} + X_{An}}{X^{\infty}_{Ap} + X^{\infty}_{An}}\right) \tag{8}$$

If the fraction of segments in the polar state in the bulk solution is denoted by p, and the fraction of nonpolar segments in the bulk by n, then

$$p = \frac{X^{\infty}_{Ap}}{X^{\infty}_{Ap} + X^{\infty}_{An}} \tag{9}$$

$$n = \frac{X^{\infty}_{An}}{X^{\infty}_{Ap} + X^{\infty}_{An}} \tag{10}$$

so that the equation for the free segment distribution of segments of type A becomes

$$G_A(z) = p\exp[-u_{Ap}(z)] + n\exp[-u_{An}(z)] \tag{11}$$

where

$$u_{Aj}(z) = u'(z) + \sum_{B}\sum_{k}^{p,n}\chi_{Aj,Bk}\,[\langle\phi_{Bk}(z)\rangle - \phi^{\infty}_{Bk}] \tag{12}$$

In this equation the volume fraction of each segment polarity type, $\phi_{Bk}(z)$, has been used to calculate the interaction energy. This can be evaluated using

$$\phi_{Bp}(z) = \frac{p\exp[-u_{Bp}(z)]}{p\exp[-u_{Bp}(z)] + n\exp[-u_{Bn}(z)]}\phi_b(z) \tag{13}$$

for the polar conformation, with a similar equation being obtained for $\phi_{Bn}(z)$. Using these modified equations amounts to treating each state of each segment as a "polarity" type, so that a numerical algorithm similar to that described in paper 1[8] can be used, substituting segment types with polarity types. An additional simple iteration is required to find the polar and nonpolar fractions from the bulk volume fractions using eqs 9 and 10. The iterations were carried out using a modified Newton's method, and the calculations were performed on a Sun Sparcstation 2 (Sun Microsystems).

Once the volume fraction profiles of all segment polarity types are known, then the translationally restricted excess free energy can be calculated using a slightly modified form of the equation presented by Hurter et al.:[8]

$$\frac{A^{\sigma}}{kT} = -\sum_{i=1}^{c}\theta_i^{exc} - \sum_{z=1}^{M}L(z)\frac{u'(z)}{kT} - \frac{1}{2}\sum_{A'}\sum_{B'}\sum_{z=1}^{M}\chi_{A',B'}L(z)\,[\phi_{A'}(z)\,\langle\phi_{B'}(z)\rangle - \phi^{\infty}_{A'}\phi^{\infty}_{B'}] \tag{14}$$

where A′ and B′ represent polarity types rather than segment types. The translationally restricted free energy of micelle formation can thus be calculated as a function of aggregation number, which leads to the generation of a stability curve, as explained in detail in paper 1.[8] The conditions for stable equilibrium are derived using small system thermodynamics[17] and are given by

$$\begin{aligned} A^{\sigma} &\geq 0 \\ \partial A^{\sigma}/\partial n_{agg} &< 0 \end{aligned} \tag{15}$$

Parameter Evaluation. The parameters to be determined are the χ-parameters between all possible states of each component, the differences in internal energy between the polar and nonpolar states of both PEO and PPO, and the ratios of their degeneracies. The polycyclic aromatic hydrocarbons were modeled as chains of benzene rings; the interaction parameters between benzene and the micellar components listed in Table II are those used in paper 1.[8] The difference in the interaction between benzene and the polar and nonpolar states of the polymer segments was not accounted for in this study. Karlstrom[13] determined a set of parameters which allowed the phase behavior of PEO in water to be reproduced semiquantitatively for chains of length N = 50, 330, and 23 200 monomer units; these are listed in Table III. We have also compared the results of the model for chains with N = 68 and N = 114, using these parameters, to the binary phase diagrams of PEO in water reported by Malcolm and Rowlinson.[18] The results are illustrated in Figure 2a, where again the phase diagram is reproduced semiquantitatively.

Linse and Bjorling[16] used the phase data of Malcolm and Rowlinson[18] for PPO with a molecular weight of 400 to find suitable parameters for the PPO–W system. The

Table II. χ-Parameters for Interactions between Benzene and Micellar Components[7]

component	χ_{AB}
benzene–water	5.5
benzene–PEO	0.14
benzene–PPO	0.1

Table III. Interaction and Energy Parameters Used by Karlstrom[13] and by Linse and Bjorling[16] and the Modified Parameters for EO–PO Interactions Obtained by Comparing Data for Interfacial Tension between PEO and PPO Oligomers[19] to the Theoretical Predictions[a]

	Karlstrom's and Linse's param	modified param
$kT\chi_{EOp\text{-}EOn}$	1.266	
$kT\chi_{EOp\text{-}POp}$	0	0.4
$kT\chi_{EOp\text{-}POn}$	1.3	1.6
$kT\chi_{EOp\text{-}W}$	0.6508	
$kT\chi_{EOn\text{-}POp}$	1.3	1.6
$kT\chi_{EOn\text{-}POn}$	0	0.4
$kT\chi_{EOn\text{-}W}$	5.568	
$kT\chi_{POp\text{-}POn}$	1.4	0.4
$kT\chi_{POp\text{-}W}$	1.7	
$kT\chi_{POn\text{-}W}$	8.5	
$\Delta\tilde{u}_{EO}$	5.086	
$\Delta\tilde{u}_{PO}$	11.5	
g_{EOn}/g_{EOp}	8	
g_{POn}/g_{POp}	60	

[a] The polar and nonpolar conformations of PEO are represented by EOp and EOn, respectively, and similarly the conformations of PPO are represented by POp and POn. Water is denoted by W. The difference in internal energy between the polar and nonpolar conformations is denoted $\Delta\tilde{u}_i$, and g_{EOn}/g_{EOp} is the ratio of degeneracies for the polar and nonpolar conformations. The energy and interaction parameters are reported in kJ/mol.

predictions of the model and the experimental results are compared in Figure 2b, for the PPO–W parameters listed in Table III. Linse and Bjorling used these parameters, and those for the PEO–W system reported by Karlstrom, to predict successfully the adsorption of a Pluronic polymer from aqueous solution as a function of temperature. For these calculations the interaction parameters between PEO and PPO were also required, and the parameters they used are listed in Table III. We attempted to reproduce the data for the interfacial tension between PEO and PPO oligomers of Bailey et al.[19] using these parameters and were unable to achieve phase separation between the PEO and PPO. Using the modified parameters listed in Table III, the model was able to predict the phase separation of PEO and PPO oligomers, as illustrated in Figure 2c. The theory agrees with the experimental finding that no phase separation occurs for ethylene oxide with a chain length of 10 units. Parameters were chosen which agreed with the experimental value for the interfacial tension at long chain lengths where end effects (resulting from the terminal hydroxyl group on the PEO chain and the terminal methyl group on the PPO chain) would be less important. To avoid attempting to fit multiple parameters with a limited amount of data, it was assumed that the interactions between EO and PO are symmetric, as shown in Table III.

Bjorling et al.[20] have provided some direct evidence for Karlstrom's model by measuring the ^{13}C NMR chemical shift of the methylene carbons in PEO as a function of temperature and solution composition. The polar conformation gives rise to a lower average chemical shift than does the nonpolar conformation. Using Karlstrom's model to find the fraction of polar conformations, Bjorling et al. calculated the expected shift as a function of temperature and solution composition and found semiquantitive agreement between the experimental NMR results and the theoretical predictions.

The Karlstrom model thus appears to reproduce both the phase behavior and conformational changes of the PEO–W system satisfactorily. Though fewer experimental results are available for the PPO–W and PEO–PPO system, the model appears to describe these systems equally well.

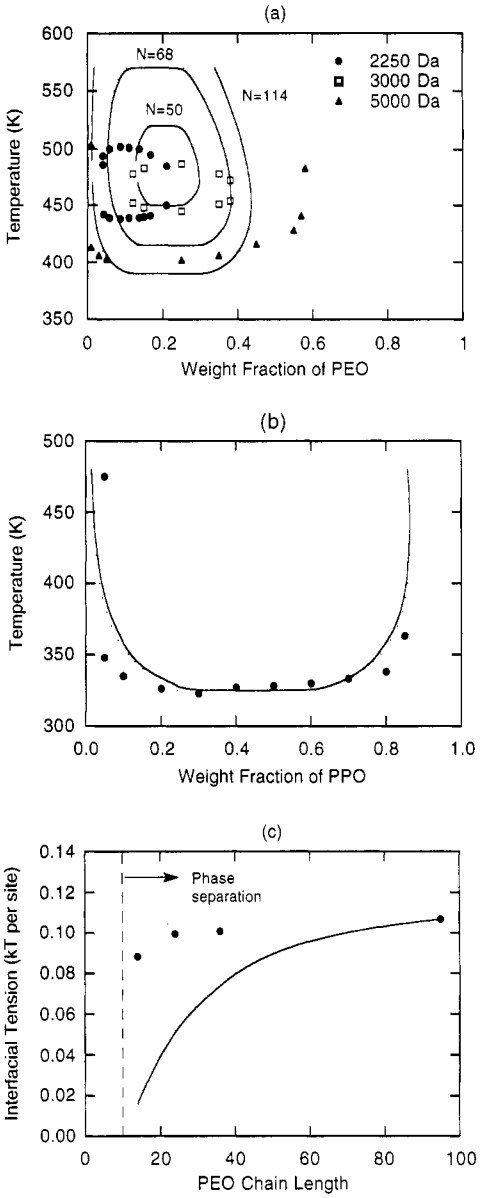

Figure 2. Parameter estimation from the phase behavior of PEO, PPO, and water systems. (a) Comparison of experimental PEO–W phase diagrams,[18] and the theoretical predictions using Karlstrom's model.[13] (b) Experimental phase diagram of PPO (MW = 400) in water,[18] compared with model predictions using the parameters listed in Table III. (c) Interfacial tension data for PEO–PPO oligomers[19] compared with model predictions, using the modified parameters in Table III. The PO molecular weight was 2000; the interfacial area per lattice site was 18 Å^2; $T < 346$ K.

Results

The self-consistent mean-field theory allowing for a distinction between polar and nonpolar states of individual polymer segments presented here has been used to explore the effects of temperature and solubilizate concentration on the aggregation properties of block copolymers of different composition, architecture, and molecular weight. We discuss first the micellization behavior, and then extend this discussion to consider also the interaction between solubilization and micelle structural characteristics.

Micelle Formation. Figure 3 shows the predicted micellar profiles for a triblock copolymer, $EO_{30}PO_{61}EO_{30}$, representing the Pluronic polymer P104. When compared with the lattice theory for flexible-chain molecules,[8] the two-state model predicts the formation of smaller micelles, with a higher water content and lower PPO content in the core. This is a direct result of allowing the PPO and PEO

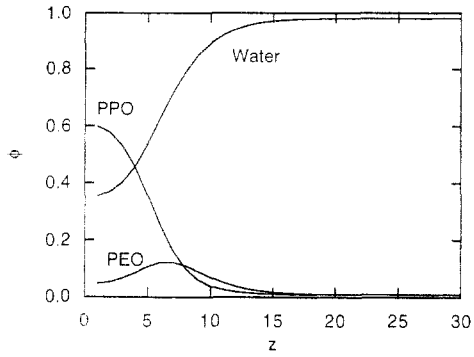

Figure 3. Micellar profiles for $EO_{30}PO_{61}EO_{30}$ (Pluronic P104) for an average polymer volume fraction of 0.04 and T = 310 K.

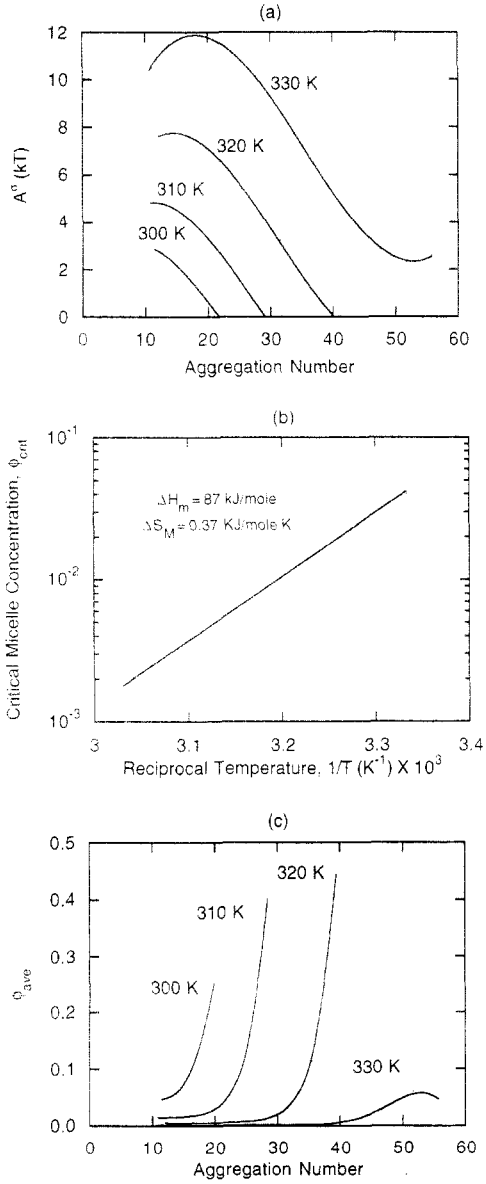

Figure 4. Temperature effect on (a) the stability curve, in terms of the excess free energy of a translationally restricted micelle as a function of aggregation number, (b) the critical micelle concentrations, and (c) the overall polymer volume fraction as a function of the aggregation number, for P104 micelles.

chains to adopt two different states, one polar and the other nonpolar, and has important ramifications with regard to solubilization characteristics, as discussed later.

The temperature dependence of the aggregation behavior of P104 is illustrated in Figure 4. The stability curves in Figure 4a indicate that with increasing temperature the aggregation number of the micelles increases. The higher the value of A^σ at the onset of aggregation (the maximum on the curve), the lower the polymer concentration. Thus the critical micelle concentration (cmc) decreases upon raising the temperature; this is shown explicitly in Figure 4b, where it is observed that the logarithm of the critical micelle concentration (expressed as a mole fraction) increases linearly with reciprocal temperature. From the slope and intercept of this plot, estimates of ΔH_m and ΔS_m, the enthalpy and entropy of micellization, respectively, can be made. We obtain ΔH_m = 87 kJ/mol and ΔS_m = 0.37 kJ/mol·K, values which are approximately 30% of those obtained experimentally: ΔH_m = 295 kJ/mol and ΔS_m = 1.05 kJ/mol·K.[21] This agreement is expected to improve with updated estimates for the interaction parameters in the model as they become available. These results also emphasize that the micellization process is endothermic and is strongly entropically-driven.

At 330 K, the polymer has become sufficiently hydrophobic that spherical micelles do not form at all compositions. This is evident from the results shown in Figure 4a, where the minimum in A^σ is greater than zero; this corresponds to a volume fraction considerably less than unity. There are two possible reasons for this observation. First, at high polymer concentrations, as the temperature is raised and the cloud point of the polymer is reached, phase separation could occur. Alternatively, it is likely that the polymer structure is such that it cannot sustain spherical micelles, and micellar growth leads to the formation of, e.g., cylindrical structures, which were not accounted for in the calculations.

Figure 4c shows that the aggregation number increases rapidly with polymer concentration in the dilute regime, but at concentrations far from the cmc the aggregation number is approximately invariant with a change in the polymer concentration. Again it is evident that at 330 K the micelles become very large at low polymer concentrations, and either phase separation or micellar growth probably occurs once the spherical micelles become unstable.

The stability curves of the Pluronic polymers P103, P104, and P105 at 310 K are compared in Figure 5. For higher PEO contents (e.g., F108, which contains 80% PEO), the polymers are not sufficiently hydrophobic to form micelles at this temperature but do form micelles at higher temperatures. From this figure, it can be concluded that raising the PPO content of the polymer increases the aggregation number and decreases the cmc. The most hydrophobic polymer (P103) does not form spherical micelles at higher polymer concentrations owing to precipitation or phase separation, or to the formation of other, more energetically-favored, micellar structures such as cylinders or lamellae. The effect of polymer composition on the critical micelle concentration is shown in Figure 5b for a temperature of 310 K and constant size of the hydrophobe. Clearly, the more hydrophobic polymers show a greater propensity to form micelles, as evidenced by their lower cmc's. This behavior, of course, is not unexpected.

The hydrophobicity of a polymer increases with molecular weight, which increases the tendency for the polymers to aggregate. Figure 6 shows the molecular weight effect on the stability curves of Pluronic polymers with 40 wt % PEO. The lowest molecular weight polymer does not show any tendency to form stable micelles (since $\partial A^\sigma/\partial N_{agg} > 0$). As the molecular weight increases, an inflection in the curve develops, and at higher molecular weights stable micelles are formed. As the molecular

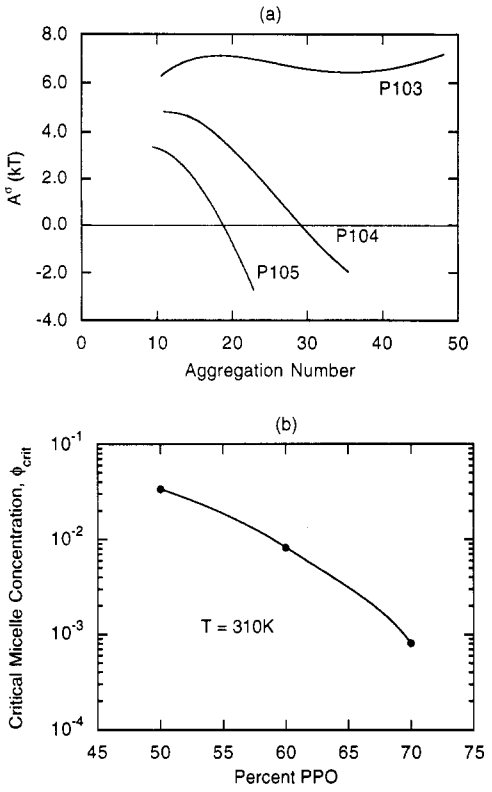

Figure 5. Effect of block copolymer composition on (a) the stability curves and (b) critical micelle concentrations, for Pluronic polymers of constant PPO content and varying ethylene oxide content at 310 K.

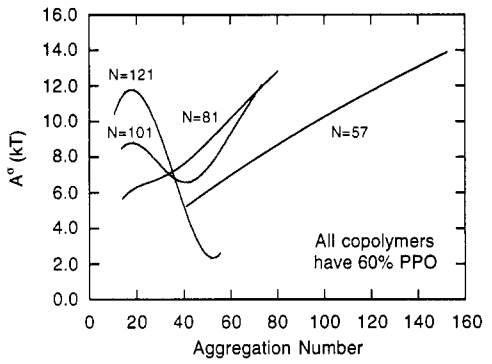

Figure 6. Molecular weight effect on the stability curves of triblock copolymers wiht 40 wt % PEO, at 330 K. N is the total number of segments in a polymer chain.

weight increases, the cmc decreases (as is evident from the increase in the peak values of A^σ), and the range of polymer concentrations over which micelles can form increases.

Figure 7 shows the effect of temperature on the structure of $EO_{25}PO_{51}EO_{25}$ micelles. This polymer has the same composition as P104 but a lower molecular weight. Stability curves (not shown) indicate that the effect of temperature is similar to that observed for P104; raising the temperature decreases the cmc and increases the aggregation number of the micelle for a given polymer concentration. Figure 7a compares the segment density profiles for micelles formed by this polymer at 325 and 330 K; at the higher temperature, the micelle is slighly larger, the concentration of PPO in the core is higher, and the water concentration is lower. The hydrophobicity of the core thus increases with an increase in temperature, which would increase the affinity of the micelle for nonpolar solutes. The probability distribution of segments in the polar state in the micelle shown in Figure 7b clearly demonstrates that the conformation of the polymer is

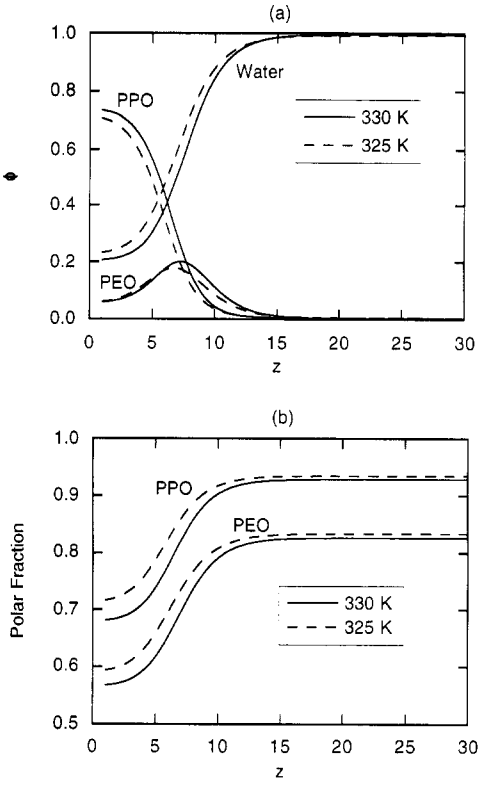

Figure 7. Structure of $EO_{25}PO_{51}EO_{25}$ micelles at 325 and 330 K: (a) segment density profiles and (b) fraction of polymer segments in the polar conformation as a function of position in the micellar solution, for a total polymer volume fraction of 0.01.

affected by both the temperature and the composition of the surrounding solution, so that both PEO and PPO have a lower fraction of polar segments in the core of the micelle than in the bulk solution, and the polar fraction decreases with an increase in temperature. Similar effects are obtained for the branched Tetronic polymers.

The effects of polymer structure on the stability curves and micellar profiles are shown in Figure 8. The stability curves for diblock copolymers, triblock copolymers (Pluronics), polymers with three branches, and polymers with four branches (Tetronics), all having the same overall molecular weight and composition, are compared in Figure 8a. It is clear that the polymer architecture plays a significant role in the micellization behavior. As the number of branches is increased, micelles with lower aggregation numbers are formed, with dramatic increases in the cmc. The segment density profiles for micelles formed by these polymers are shown in Figure 8b. Clearly, the more complex the structure, the smaller is the micelle that is formed. The reason for this behavior is related to the changes in the number of favorable configurations a polymer of a given structure can take on. For instance, the free ends of the hydrophobic blocks of the diblock copolymers are free to sample the entire apolar core region, while for the triblock copolymers both ends of the hydrophobe are constrained to be near the interfacial region, as they are attached to the corona-forming hydrophilic groups. This then restricts the degree to which the hydrophobes can extend into the apolar core and mix with each other, resulting in smaller core regions. As the degree of branching increases, the configurational constraints become more severe, and even smaller micelles result. In addition to this, it can be argued that the core radius cannot exceed the length of the PPO block. Branching at overall constant composition leads to a shorter PPO block and thus a smaller maximum core size.

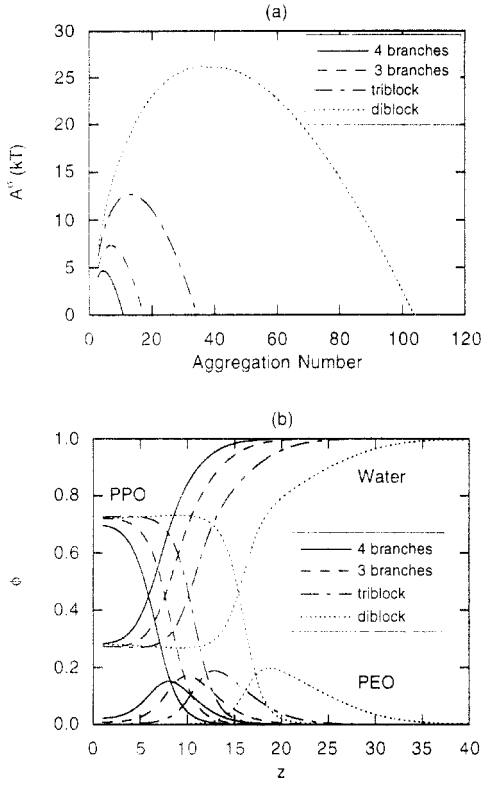

Figure 8. Effects of polymer structure on micelle properties for a constant molecular weight of N=241, at 300 K: (a) stability curves and (b) micellar profiles.

Solubilization. The effects of naphthalene solubilization on the properties of the block copolymer solution are shown in Figure 9. The segment density profiles for a P104 micelle with solubilized naphthalene are compared with those for a solute-free micelle at the same polymer concentration in Figure 9a. The naphthalene, which is confined chiefly to the core of the micelle, causes it to become larger, with a lower core concentration of water and a higher concentration of PPO. The presence of the solute thus has a major effect on the micelle structure; indeed, the micelle aggregation number increases with an increase in the naphthalene bulk concentration and hence with solute uptake, as illustrated in Figure 9b. This is in agreement with the experimental results of Al-Saden et al.,[1,2] who found that the increase in the hydrodynamic radius of L64 aggregates with hexane uptake was greater than could be explained by the additional volume of the solute and attributed it to an increase in the aggregation number.

Because of these significant changes in the micelle structure, in which larger micelles with a larger and more hydrophobic core are formed, it cannot be expected that the micelle–water partition coefficient (defined as the ratio of solute concentration in the micelle to that in the bulk solution) will remain constant as the solute bulk concentration is increased. This is indeed the case, as illustrated in Figure 9c, where there is clearly a strong effect of bulk concentration on the partition coefficient. Similar results have been noted by Cogan et al.[10] in their study of inverse block copolymer systems, where the continuous phase is an organic solvent, while the solute is water.

Finally, as the naphthalene loading is increased, the solute bulk concentration initially increases, but at high naphthalene loadings the bulk solution becomes saturated. Above the saturation point, the excess naphthalene will precipitate, and there will be no further uptake by the micelle. The core will be a saturated solution of naphthalene and PPO segments with small amounts of water

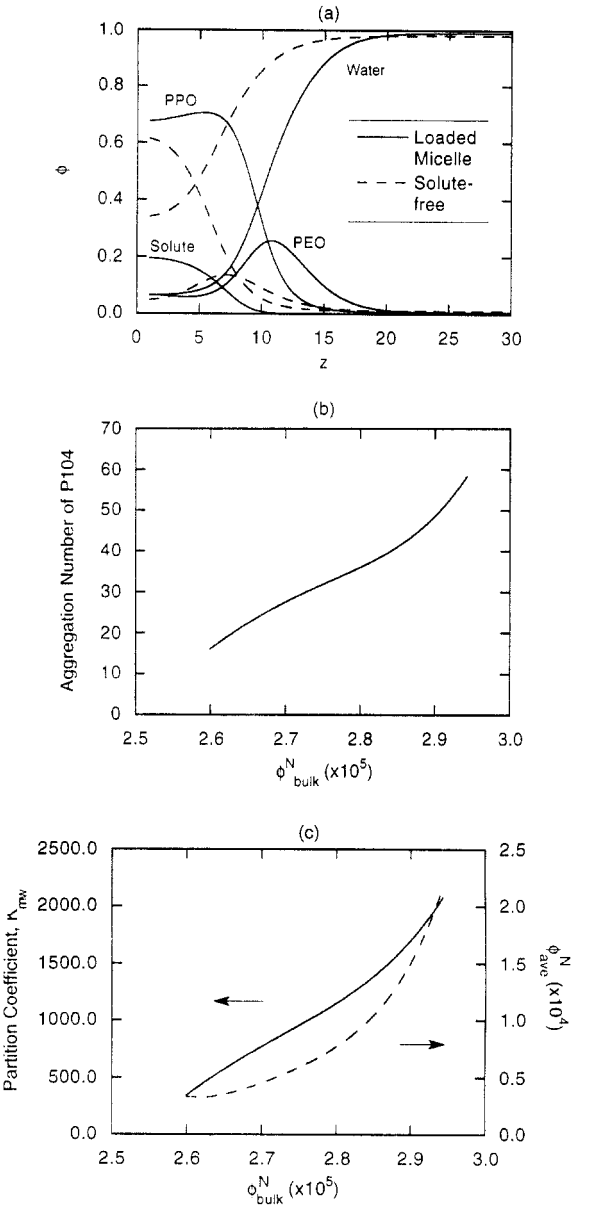

Figure 9. Effect of solute uptake on micellization and solubilization properties of $EO_{30}PO_{61}EO_{30}$ (Pluronic P104) at 300 K. (a) Segment density profiles for micelles with and without solubilized naphthalene. The micelle with solubilized naphthalene is close to the saturation point. The average polymer volume fraction is 0.05 in both cases. (b) Increase in the aggregation number of P104 micelles with an increase in the naphthalene bulk concentration, for a polymer volume fraction of 0.01. (c) Solubilization of naphthalene in micelles as a function of naphthalene bulk concentration and variation in the partition coefficient. The polymer volume fraction is 0.01.

present. The volume fraction of naphthalene in the bulk at saturation predicted by the model is 2.95×10^{-5}, which is close to the value 3.5×10^{-5} calculated from the solubility of naphthalene in water[22] and the molar volume of naphthalene. For lower molecular weight solutes which exist as liquids in the pure state, the phase separation can be expected to take place within the micellar cores, leading to the formation of small microemulsion droplets.

The concentration of naphthalene in the solution surrounding the micelles, referred to here as the naphthalene *bulk concentration*, is not exactly equal to the concentration of naphthalene in pure water that would be in equilibrium with the micelles themselves, due to the presence of unaggregated polymer in the bulk solution, which associates with the naphthalene to some extent and increases in solubility. At equilibrium, the equality of the

solute activities (or the chemical potentials) in the micellar solution and in pure water can be used to find that concentration of naphthalene in water, ϕ_N^W, with which the micellar solution (both micelles *and* bulk solution) would be in equilibrium. The chemical potential of component j in a multicomponent mixture of block copolymers is derived by minimizing the free energy (eq 14) with respect to the number of molecules of j:[23,24]

$$\frac{\mu_j - \mu_j^*}{kT} = \ln \phi_j + 1 - r_j \sum_i \frac{\phi_i}{r_i} - \frac{r_j}{2} \sum_{A',B'} (\phi_{A'} - \phi_{A'j}^*)\chi_{A'B'}(\phi_{B'} - \phi_{B'j}^*) \quad (16)$$

The reference state μ_j^* refers to a hypothetical state of pure amorphous component j, and $\phi_{A'j}^*$ and $\phi_{B'j}^*$ are the volume fractions of polarity types A′ and B′ in pure component j. The second summation is over all polarity types, i.e., both polar and nonpolar segment types, as in eq 14.

Figure 10a shows the naphthalene bulk concentrations in 10% solutions of P104, P105, and P106, compared to the equilibrium concentration of naphthalene in pure water. P104 and P105 model the Pluronic polymers of the same name, and P106 is a hypothetical polymer (EO_{50}-$PO_{61}EO_{50}$), with 55% PEO, and the same molecular weight of PPO as P104 and P105. The concentration of naphthalene in the bulk solution is higher than the equilibrium water concentration because the free polymer in the bulk solution associates with the naphthalene to some degree and enhances its water solubility. The concentration of polymer in the bulk solution increases with increasing ethylene oxide content of the polymer, as shown in Figure 10b, causing an increase in the naphthalene solubility. Figure 10b also shows that the polymer bulk concentration decreases with increasing solute concentration; it appears that the addition of a hydrophobic solute increases the aggregating tendencies of the polymer, resulting in a higher aggregation number and a lower concentration of polymer in the bulk solution. The fact that the polymer bulk concentration changes with solute concentration is one of the contributing factors leading to the nonlinear relationship between the partition coefficient and the equilibrium concentration of naphthalene in water illustrated in Figure 9c, for a 1% solution of P104, and is consistent with the light scattering results of Al-Saden et al.,[2] which show that the aggregation number of the polymer increases with solute uptake.

Figure 10c also shows that the solubility of naphthalene is greater, the higher the PPO content of the polymer, which is in qualitative agreement with the results of Hurter and Hatton.[7] The relationship between the PPO content of the polymer and solubilization capacity is illustrated more clearly in Figure 11, which compares experimental results[7] and the theoretical predictions for the enhancement in the naphthalene solubility afforded by a 10% polymer solution relative to its solubility in pure water, as a function of polymer PPO content. The theory reproduces the experimental finding that there is a strong correlation between the PPO content of the polymer and its propensity to solubilize naphthalene, although it does overpredict the magnitude of the PPO effect. The agreement could probably be improved by taking such factors as the statistical segment length and the difference in molecular volumes of the individual segments into account, but this would involve introducing additional parameters which would be difficult to estimate independently and is therefore beyond the scope of this work.

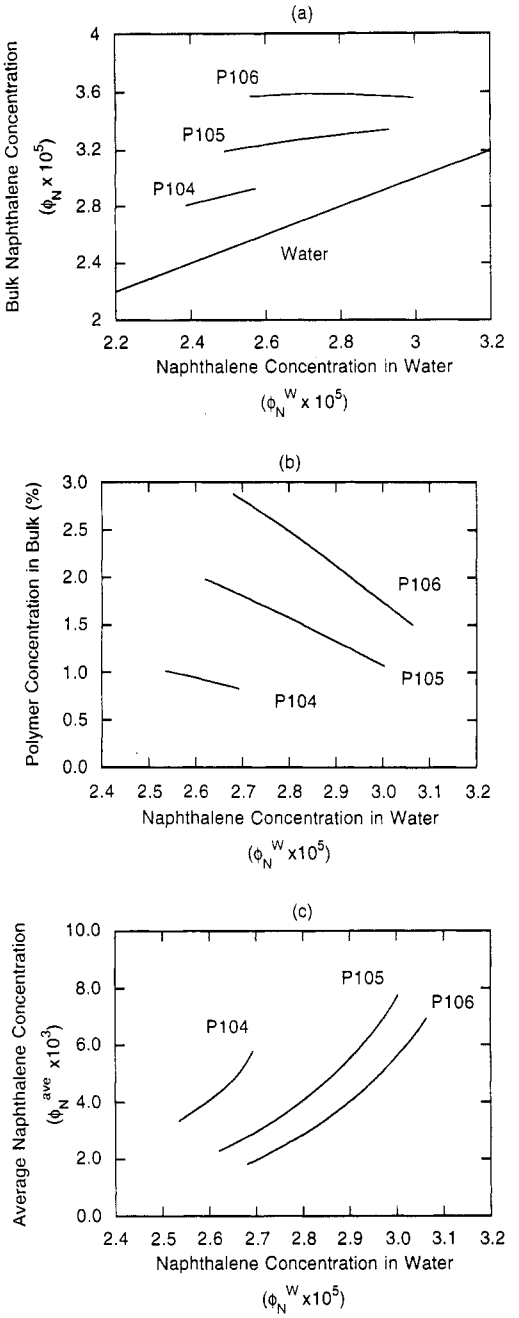

Figure 10. Effect of polymer structure on the bulk and average naphthalene concentrations in equilibrium with a pure water phase of concentration ϕ_N^W: (a) concentration of naphthalene in the bulk solution surrounding the micelles, (b) concentration of free polymer in the bulk solution surrounding the micelles, and (c) enhanced solubility of naphthalene. The naphthalene uptake increases with increasing PPO content of the polymer.

Hurter and Hatton[7] observed that the normalized partition coefficient K'_{mw} (based on the concentration of the hydrophobic PPO block concentration rather than the total polymer concentration) was not independent of polymer PPO content and suggested this might be the result of changes in the micelle structure with polymer composition. This supposition is borne out by the predictions of the theory, as is shown in Figure 12, where the micellar profiles for naphthalene solubilized in P104 and in P106 are compared. The P106 forms a smaller micelle, with a higher concentration of water and lower concentration of naphthalene in the core. The volume of the interfacial region (from which naphthalene is essentially excluded) is similar in both cases, so that the ratio of core volume to interfacial volume decreases with

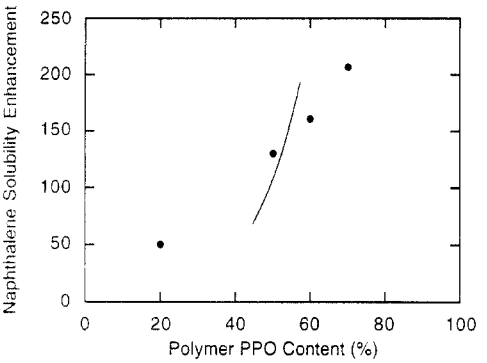

Figure 11. Effect of PPO content on the enhancement in naphthalene solubility in 10% solutions of triblock copolymers at 300 K. Experimental results are from Hurter and Hatton.[7]

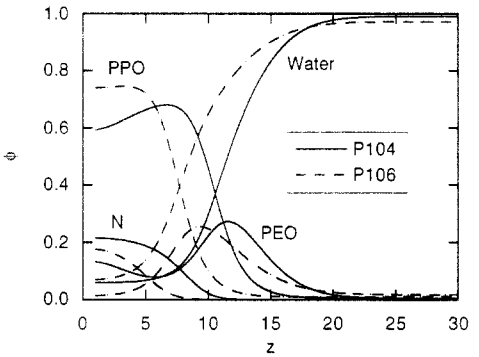

Figure 12. Micellar profiles for naphthalene solubilized in P104 and in P106 at 300 K. The average polymer composition is 10%, and the micellar solutions are in equilibrium with a volume fraction of naphthalene in water of 2.7×10^{-5}.

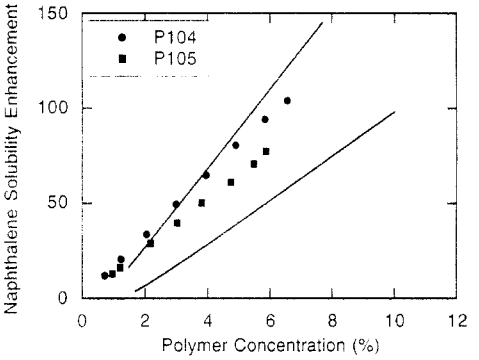

Figure 13. Comparison of experimental results for the enhanced solubility of naphthalene with an increase in polymer concentration[7] with theoretical predictions, for P104 and P105 at 300 K.

decreasing micelle size, i.e., with increasing ethylene oxide content. Since a significant amount of PPO is located in the interfacial region, the amount of PPO available to solubilize naphthalene decreases. Thus the composition of a polymer has a strong effect on the structure of the micelle, which in turn influences the solubilization behavior.

The partition coefficient has been found experimentally to be independent of polymer concentration for P104 and P105, in the concentration range 1–10% polymer.[7] As illustrated in Figure 13, model predictions agree semiquantitatively with the experimental results on the solubilization of naphthalene in P104 and P105 as a function of polymer concentration.

Thus, the theory predicts that the partition coefficient of naphthalene increases with an increase in the solute concentration owing to the changes in the structure of the micelle because of the uptake of solute: the polymer

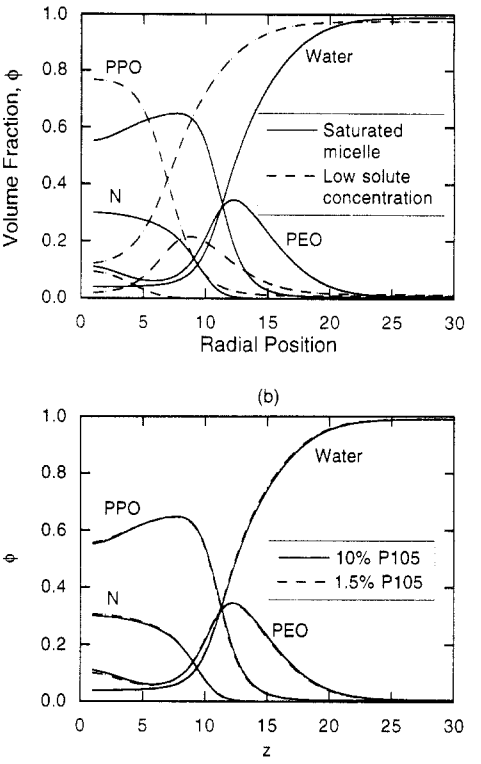

Figure 14. Naphthalene solubilization profiles in P105 block copolymer micelles: (a) comparison of profiles at low concentrations and at close to saturation with a 10% polymer solution and (b) effect of polymer concentration for a solute concentration close to saturation ($\phi_N^W = 2.7 \times 10^{-5}$).

aggregation number increases, and a more hydrophobic core is formed, with a lower water concentration and higher PPO concentration. The concentration of polymer in the bulk also decreases upon solute addition. On the other hand, an increase in the polymer concentration results in more micelles being formed, with the same aggregation number, so that for a given bulk concentration of naphthalene, the partition coefficient remains constant with an increase in polymer concentration. These conclusions are supported by the effect on the micellar profiles of solute addition and of changes in the polymer concentration, as shown in parts a and b of Figure 14, respectively. The micelles become larger as a result of the swelling due to incorporation of the solute within the micellar core, as well as to an increase in the polymer aggregation number (Figure 14a). Water is excluded from the core of the solute-saturated micelles, and the concentration of solute in the core increases. Figure 14b shows that the micellar profiles for naphthalene solubilized in 1.5% P105 and in 10% P105 are essentially indistinguishable, pointing to the lack of a polymer concentration effect on the individual micelle characteristics.

Experimentally it has been observed that the molecular weight of the polymer has a significant effect on the partitioning behavior of naphthalene in Pluronic and Tetronic polymers.[7] The lattice theory for flexible-chain molecules presented in paper 1[8] significantly underpredicted the magnitude of this effect. The modified lattice theory shows a far stronger dependence on molecular weight, as is illustrated in Figure 15a, where theoretical predictions are compared to the experimental results for Pluronic polymers. The theory overestimates the molecular weight effect somewhat, though the agreement is reasonable.

In addition to showing that naphthalene solubilization increases with polymer molecular weight, the theory is

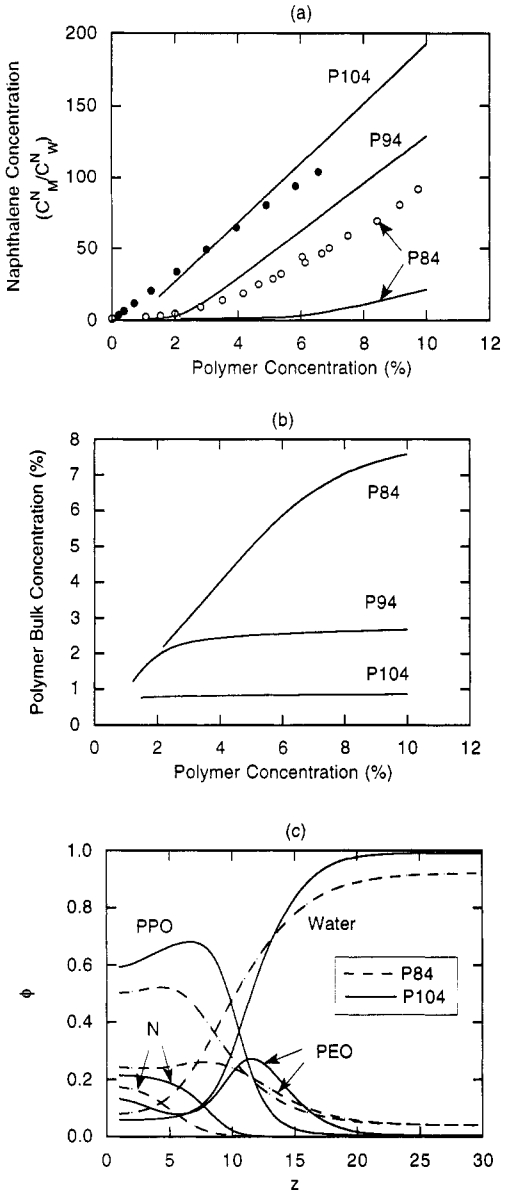

Figure 15. Effect of polymer molecular weight on the solubilization of naphthalene in block copolymer micelles: (a) experimental results for P84 and P104[7] compared to the theoretical predictions, (b) concentration of free polymer in the bulk solution surrounding the micelles, as a function of the overall polymer concentration, for three triblock copolymers with 40% PEO and differing molecular weights, and (c) comparison of the micellar profiles of naphthalene solubilized in P84 and P104.

able to reproduce the nonlinear relationship between the enhancement in naphthalene solubilization effectiveness and the polymer concentration for low molecular weight polymers that was observed experimentally with both Pluronic and Tetronic polymers by Hurter and Hatton.[7] An analysis of the theoretical results shows that the polymer bulk concentration is not constant for the low molecular weight polymers, as is illustrated in Figure 15b. For the P94, the bulk concentration initially increases but then above about 4% polymer becomes constant. This is consistent with Figure 15a, which shows that there is a linear relationship between the amount of naphthalene solubilized and the polymer concentration above 4% polymer. For the low molecular weight polymers, micelles form at a higher critical concentration (as was shown in Figure 6), and micelle properties change near the critical micelle concentration but are essentially constant far from it. This effect is even more pronounced for P84. Figure 15b also shows that the bulk polymer concentration is higher for lower molecular weight polymers, implying that less of the polymer aggregates to form micelles, which decreases the capacity of the polymer solution for naphthalene.

Finally, the micellar profiles for naphthalene solubilized in P104 and in P84 are compared in Figure 15c. The lower molecular weight polymer forms a smaller micelle, with a large interfacial region, and a heterogeneous core with a high PEO and water content. The core environment is thus much less hydrophobic for the lower molecular weight polymer, resulting in significantly less solubilization of naphthalene. This figure also shows the higher concentration of polymer in the bulk solution, which results in less polymer being available to form micelles.

Conclusion

The modification of the simple lattice theory for flexible-chain molecules to allow for polar and nonpolar conformations of the PEO and PPO chains presented here enables the theory to reproduce successfully the anomalous phase behavior of these polymers and improves the ability of the theory to predict more subtle effects such as the molecular weight dependence of naphthalene solubilization in block copolymer micelles. This improvement results from the sensitivity of the equilibrium chain conformations to both solution composition and temperature.

The theory shows that, as the temperature is increased, the fraction of segments in the nonpolar conformations increases, increasing the hydrophobicity of the polymer. This leads to exclusion of water from the core of the micelle as the temperature is raised, creating a more hydrophobic environment attractive to organic solutes. This is in agreement with the experimental results of Hurter,[9] which show an increase in solubilization of naphthalene with temperature. It also supports the observations of Al-Saden et al.,[12] who found that raising the temperature leads to a decrease in the hydrodynamic radius of the micelle, which they postulated was due to the expulsion of water at higher temperatures.

Comparison of the segment density profiles of naphthalene-saturated micelles formed by block copolymers of differing composition shows that the micelle structure is strongly dependent on the composition of the polymer. Polymers with a higher proportion of the hydrophilic block, PEO, tend to form smaller micelles, with a lower concentration of PPO and a higher concentration of water in the core, which results in less naphthalene being solubilized. The amount of naphthalene solubilized is thus not simply dependent on the amount of PPO in the solution but depends on the polymer structure and composition. Similarly, polymers of low molecular weight form micelles with a less hydrophobic core environment and are not as efficient as solubilizing naphthalene. Increasing the PEO content, or decreasing the molecular weight of the polymer, also tends to raise the concentration of free polymer in the bulk solution. This polymer is essentially wasted, since, although it enhances the solubility of naphthalene in the bulk solution to a small extent (about 2-10%), it does to a much lesser degree than the aggregated polymer, where increases in solubilization can be greatly in excess of 1000%.

The lattice theory has thus been successful in elucidating the underlying structural effects which lead to the complex solubilization behavior of polycyclic aromatic hydrocarbons in block copolymer micelles. There are some experimental systems which the theory appears unable to reproduce (for example, P103), and it would be interesting to see whether allowing the micelles to adopt other

geometries, such as cylinders and lamellar layers, would resolve these difficulties. The modified lattice theory has also shown that the micelle properties are strongly dependent on the solute concentration, whereas the only experimental results that were available for comparison were for saturated micelles. Thus further experimental characterization of these systems is warranted.

Acknowledgment. This work was funded by the M.I.T. Sea Grant College Program, under Federal Grant Number NA90-AA-SG-D424 from the National Sea Grant College Program, from the National Oceanic and Atmospheric Administration, U.S. Department of Commerce. Addition funding was provided by Union Carbide as matching funds for an NSF Presidential Young Investigator Award to T.A.H., by a Charles E. Reed Initiation Award, and by the Department of Energy under Grant Number DE-FG02-92ER14262. We are grateful to Frans Leermakers and Gerard Fleer for their critical reading of the original manuscript and suggestions for improving the clarity of the paper.

References and Notes

(1) Al-Saden, A. A.; Florence, A. T.; Morrison, H.; Whateley, T. L. *J. Pharm. Pharmacol. Suppl. (Br. Pharm. Conf. 1979)* **1979**, *31*, 81P.
(2) Al-Saden, A. A.; Whateley, T. L.; Florence, A. T. *J. Colloid Interface Sci.* **1982**, *90*, 303–309.
(3) Brown, W.; Schillen, K.; Almgren, M.; Hvidt, S.; Bahadur, P. *J. Phys. Chem.* **1991**, *95*, 1850–1858.
(4) Cowie, J. M. G.; Sirianni, A. F. *J. Am. Oil Chem. Soc.* **1966**, *43*, 572–575.
(5) McDonald, C.; Wong, C. K. *J. Pharm. Pharmacol.* **1974**, *26*, 556–557.
(6) Zhou, Z.; Chu, B. *J. Colloid Interface Sci.* **1988**, *126*, 171–180.
(7) Hurter, P. N.; Hatton, T. A. *Langmuir* **1992**, *8*, 1291–1299.
(8) Hurter, P. N.; Scheutjens, J. M. H. M.; Hatton, T. A. *Macromolecules*, in press.
(9) Hurter, P. N. Ph.D. Thesis, Massachusetts Institute of Technology, Cambridge, MA, 1992.
(10) Cogan, K. A.; Leermakers, F. A. M.; Gast, A. P. *Langmuir* **1992**, *8*, 429–436.
(11) Leermakers, F. A. M.; Scheutjens, J. M. H. M. *J. Chem. Phys.* **1988**, *89*, 3264.
(12) Barneveld, P. A. Ph.D. Thesis, Wageningen Agricultural University, Wageningen, The Netherlands, 1991.
(13) Karlstrom, G. *J. Phys. Chem.* **1985**, *89*, 4962–4964.
(14) Linse, P.; Malmsten, M. *Macromolecules* **1992**, *25*, 5434–5439.
(15) Linse, P. *Macromolecules* Submitted for publication.
(16) Linse, P.; Bjorling, M. *Macromolecules* **1991**, *24*, 6700–6711.
(17) Hall, D. G. In *Nonionic Surfactants*; Schick, M. J., Ed.; Marcel Dekker: New York, 1987; Vol. 23, pp 233–296.
(18) Malcolm, G. N.; Rowlinson, J. S. *Trans. Faraday Soc.* **1957**, *53*, 921–931.
(19) Bailey, A. I.; Saleme, B. K.; Walsh, D. J.; Zeytountsian, A. *Colloid Polym. Sci.* **1979**, *257*, 948–952.
(20) Bjorling, M.; Karlstrom, G.; Linse, P. *J. Phys. Chem.* **1991**, *95*, 6706–6709.
(21) Alexandridis, P.; Holzwarth, J. F.; Hatton, T. A. Work in progress.
(22) May, W. E.; Wasik, S. P.; Freeman, D. H. *Anal. Chem.* **1978**, *50*, 997–1000.
(23) Evers, O. A.; Scheutjens, J. M. H. M.; Fleer, G. J. *Macromolecules* **1990**, *23*, 5221–5233.
(24) Evers, O. A. Ph.D. Thesis, Wageningen Agricultural University, Wageningen, The Netherlands, 1990.